Published in final edited form as:
Nat Phys. 2015 October ; 11(10): 839–843. doi:10.1038/nphys3423.

Polar Pattern Formation in Driven Filament Systems Require Non-Binary Particle Collisions

Ryo Suzuki[1], **Christoph A. Weber**[2,3], **Erwin Frey**[3], and **Andreas R. Bausch**[1,4]

[1]Lehrstuhl für Biophysik (E27), Technische Universität München, 85748 Garching, Germany

[2]Max Planck Institute for the Physics of Complex Systems, Nöthnitzer Str. 38, 01187 Dresden, Germany

[3]Arnold Sommerfeld Center for Theoretical Physics and Center for NanoScience, Department of Physics, Ludwig-Maximilians-Universität München, 80333 Munich, Germany

Abstract

Living matter has the extraordinary ability to behave in a concerted manner, which is exemplified throughout nature ranging from the self-organisation of the cytoskeleton to flocks of animals [1–4]. The microscopic dynamics of constituents have been linked to the system's meso- or macroscopic behaviour *in silico* via the Boltzmann equation for propelled particles [5–10]. Thereby, simplified binary collision rules between the constituents had to be assumed due to the lack of experimental data. We report here experimentally determined binary collision statistics by studying the recently introduced molecular system, the high density actomyosin motility assay [11–13]. We demonstrate that the alignment effect of the binary collision statistics is too weak to account for the observed ordering transition. The transition density for polar pattern formation decreases quadratically with filament length, which indicates that multi-filament collisions drive the observed ordering phenomenon and that a gas-like picture cannot explain the transition of the system to polar order. The presented findings demonstrate that the unique properties of biological active matter systems require a description that goes well beyond a gas-like picture developed in the framework of kinetic theories.

Unlike animals that possess interactions such as spatial cognition or hierarchical dispositions [14–16], the interactions of reconstituted [11–13,17,18] or synthetic [19–22] model systems stem purely from physical interactions among the constituents. Although weak alignment forces have been proposed to be sufficient for the polar ordering transitions [11], no experimental data are available that quantify the interaction rules between the constituents. Due to the lack of experimental data for such interaction rules, microscopic studies assume

[4]Corresponding and requests for materials should be addressed to A.R.B.

Author contribution

R.S., C.A.W., E.F. and A.R.B. designed the project. R.S. and A.R.B. performed and designed all experiments. C.A.W. and E.F. theoretically analysed the experimental data. All authors participated in interpreting the experimental and theoretical results and in writing the manuscript.

Competing financial interests

The authors declare no competing financial interests.

Europe PMC Funders Author Manuscripts

either an average rule over the particles in the neighbourhood [23, 24] or that all binary interactions lead to perfect polar alignment [5].

Here we provide the angle resolved binary collision statistics for a paradigmatic experimental active system; the actomyosin motility assay. The experimental system consists of only two main components: actin filaments and non-processive motor proteins heavy-meromyosin (HMM) [11–13, 25]. Actin filaments move on a lawn of HMM by consumption of adenosine triphosphate (ATP) at a constant speed of approximately $4\mu m/s$, which is ensured in the experiment by using high ATP concentrations. The orientation of a single filament motion is determined solely by the head and the motion itself displays no longterm directionality, where the randomness of the system is generated by the pushing of the motors.

To obtain the binary collision statistics, the experiments are conducted under dilute conditions with filament densities between $0.005\rho_c$ and $0.06\rho_c$, where $\rho_c \approx 5$ filaments/μm^2 is the critical density for the disorder-order transition [11]. Only short filaments $L = 2 - 5\mu m$ are considered to ensure that collisions are binary and also that the collision angles can be unambiguously defined, which becomes difficult for longer filaments due to the intrinsic bending of the filaments. When two filaments encounter each other, for the majority of the collision events filaments readily cross each other. Despite the frequent crossing events we observe various tendencies in the binary collisions: polar alignment, anti-polar alignment and events where the filament orientation hardly changes (Figs. 1a–c). To quantify these tendencies we measure the incoming angle $\theta_{12} = \theta_1 - \theta_2$ along with the outgoing angle $\theta'_{12}=\theta'_1 - \theta'_2$ (Fig.1d; see Methods). Binary collisions alone are extracted and all non-binary collisions are neglected. All filament densities in the dilute regime demonstrate similar quantitative behaviour for the experimentally obtained binary collision statistics $\theta'_{12}(\theta_{12})$ (Fig. 2a), where unaffected collisions, $\theta'_{12}=\theta_{12}$, are represented by a diagonal line in the diagram. The similarity in the behaviours indicates that there are no significant spatial correlations between the filaments for the dilute densities considered.

The distribution $P(\theta_{12})$ of the incoming angle exhibits an asymmetric shape which is consistent with the Boltzmann scattering cylinder for rods [8, 9] when considering the assumption of slender rods (Supplementary Information), which gives $P(\theta_{12}) \propto \Gamma(\theta_{12}) = 2L v_0 |\sin(\theta_{12}/2)| \cdot |\sin\theta_{12}|$ (see red line in Fig. 2b). Here, L denotes the filament length and v_0 is the filament speed. The limiting case of slender rods is justified since actin filaments have a length of $L = 2 - 5\mu m$ and a diameter of $d \approx 8nm$. The Boltzmann scattering cylinder Γ describes the frequency of collisions between propelled particles of constant speed as a function of the relative angle θ_{12}, which is derived by geometric considerations. Due to the large aspect ratio, incoming angles close to 0° and 180° are less likely for slender rods, and the corresponding distribution is asymmetric.

Averaging the experimentally obtained binary collision statistics $\theta'_{12}(\theta_{12})$, we see that while most events for incoming angles $\theta_{12} > 80°$ are indeed largely unaffected by the collision, at highly acute θ_{12} a clear polar bias can be recognised: θ'_{12} is smaller than θ_{12} (Fig. 2c). The

distribution of $\theta'_{12}(\theta_{12})$ is significantly skewed toward polar outcomes for highly acute θ_{12} and anti-polar outcomes for θ_{12} close to 180° (Fig. 2d). Because of this strong skewness, all data points of the experimental binary collision statistics and not just the average and standard deviation are required to make a proper prediction on the existence of transition to polar order. Using the average of the collision statistics can lead to the loss of important information concerning the collision events and can ultimately cause a wrong prediction on the existence of polar order [7].

To connect the microscopic dynamics to the meso- or macroscopic pattern formation and ordering transition in active systems, the Boltzmann equation for propelled particles has been successfully applied [5–10]. The Boltzmann equation describes the mesoscopic particle motion and maps the pre-collision states on the post-collision states, which enables the analytical prediction of the onset to polar order. It determines the time evolution of the one-particle distribution function $f(\mathbf{r}, \theta, t)$, where $\mathbf{r}$ are the coordinates, θ is the particle orientation, and t is time:

$$\partial_t f(\mathbf{r},\,\theta,\,t)+v_0\hat{\mathbf{v}}(\theta)\cdot\nabla f(\mathbf{r},\theta,t)=D_\theta\partial_\theta^2 f+C[f^{(2)}]. \quad (1a)$$

The streaming term, $v_0\hat{\mathbf{v}}(\theta)\cdot\nabla f(\mathbf{r},\theta,t)$, accounts for the movement of particles with velocity $v_0\hat{\mathbf{v}}(\theta)$, where v_0 denotes the constant speed and $\hat{\mathbf{v}}(\theta)=(\cos\theta,\sin\theta)$. Angular fluctuations are described as $D_\theta\partial_\theta^2 f$ (see Refs. [20, 26]), with D_θ denoting the angular diffusion constant. The collision integral, $C[f^{(2)}]$, captures the effect of binary filament collisions and the filament geometry. It consists a two-particle density $f^{(2)}(\mathbf{r}, \theta_1, \theta_2, t)$, which can be written in the absence of correlations as $f^{(2)}(\mathbf{r}, \theta_1, \theta_2, t) = f(\mathbf{r}, \theta_1, t)f(\mathbf{r}, \theta_2, t)$. The collision integral $C[f^{(2)}]$ plays a key role since the experimentally obtained data enter this term, which determines whether a transition to polar order exists or not. $C[f^{(2)}]$ can be divided into a loss (−) and a gain (+), $C[f^{(2)}] = C^-[f^{(2)}] + C^+[f^{(2)}]$, [7]:

$$C^-[f^{(2)}]=-\int_{-\pi}^{\pi}d\theta'\,\Gamma(\theta_{12})f^{(2)}(\theta,\theta'), \quad (1b)$$

$$C^+[f^{(2)}]=\int_{-\pi}^{\pi}d\theta_1\int_{-\pi}^{\pi}d\theta_2\frac{1}{2}\sum_{j=1}^{2}\Gamma(\theta_{12})f^{(2)}(\theta_1,\theta_2)\times\int_{-\infty}^{\infty}d\eta_j p_j\,(\eta_j|\theta_{12})\sum_{m=-\infty}^{\infty}\delta\,(\theta_j+\eta_j-\theta+2\pi m)\,,$$

(1c)

where we omitted time and space dependencies for brevity. The gain and loss contributions are derived from integrating over all possible pre-collision orientations of the particles. Each pre-collision orientation is multiplied by a frequency given by the Boltzmann collision cylinder for rods, $\Gamma(\theta_{12})$, on the post-collision angle using the definition $\theta_j \to \theta_j+\eta_j(\theta_{12})=\theta'_j$, $j\in\{1, 2\}$, where η_j denotes the change of the j-th particle orientation.

For a given relative pre-collision angle θ_{12}, the orientation of particle j changes by $\eta_j(\theta_{12})$ with probability $P_j(\eta_j|\theta_{12})d\eta_j$. The experimental scattering statistics (Fig. 2a) is equivalently expressed in terms of $P_j(\eta_j|\theta_{12})$ (Figs. 3a,b; Supplementary Information). If the filaments are indistinguishable, two important symmetry properties of p_j need to be satisfied: 1) Particle exchange symmetry $p_1(\eta_1|\theta_{12}) = p_2(\eta_2| - \theta_{12})$, 2) Mirror symmetry $p_1(-\eta_1/\theta_{12}) = p_1(\eta_1/ - \theta_{12})$, where the same argument applies for p_2. Indeed both are obeyed in the experimentally obtained binary collision statistics of the actomyosin motility assay system (Figs. 3c,d; Supplementary Information). This indicates that experimental uncertainties, such as the narrow filament length distribution, do not influence or bias the binary collision statistics.

Equation (1) is now analysed in terms of Fourier modes, where all Fourier coefficients are determined by the comprehensive binary collision statistics p_j [7]. The Fourier representation is a good starting point to derive the homogeneous and linearised equations for the coarse-grained momentum g, $\partial_t g = \nu g$. The calculation also yields the coefficients ν in terms of p_j. The equations for the momentum become unstable for $\nu > 0$, thus the transition density of polar order corresponds to $\nu = 0$ [5, 26]. Specifically, the coefficient $\nu = -D_\theta + \overline{\nu}[p_j]\rho v_0 L/\pi$, where $\overline{\nu}[p_j]$ contains the comprehensive binary collision statistics P_j (Figs. 3a,b). See Supplementary Information for the detailed mathematical expressions. Importantly, for the onset of polar order ($\nu > 0$), $\overline{\nu}$ must be positive.

Using the experimental data (Figs. 2b and 3a,b), we find $\overline{\nu} \approx -0.094$ for binning of $\Delta\theta_{12} = 15°$ and $\Delta\eta = 15°$ (see Supplementary Information for details on the computation of $\overline{\nu}$ using experimental data). The negative sign of $\overline{\nu}$ computed from the experimental data is robust against binning of η and θ (Supplementary Information). This implies that the binary collision description is insufficient to explain the ordering transition in the experimental system, for any density ρ and the isotropic state is linearly stable. This statement is independent of the value of the rotational diffusion constant D_θ since it opposes the formation of polar order, expressed by a negative sign in ν. We test the consistency of our results with analytic predictions for a well established theoretical model system where rods interact by half-angle alignment ($\eta_j = \theta_i/2 - \theta_j/2$) [5, 6], which results in $\overline{\nu} \approx 1.008$ (Supplementary Information) agreeing well with Refs. [6, 7] and thus enables the correct prediction of an order transition.

Though we show that polar order cannot be reached when neglecting angular correlations (molecular chaos), small locally aligned filament clusters could still trigger the onset of polar order by binary collisions [7, 27]. To model such weak orientational correlations we write $f^{(2)}(\mathbf{r}, \theta_1, \theta_2, t) = \chi(\theta_{12})f(\mathbf{r}, \theta_1, t)f(\mathbf{r}, \theta_2, t)$, where $\chi(\theta_{12})$ characterises the precursor angular correlations; for $\chi = 1$ angular correlations are absent leading to the assumption of molecular chaos. Led by recent studies of angular correlations in a self-propelled particle system [7], we emulate angular correlations as $\chi(\theta_{12}) = 1 + A/\theta_{12}$. A is a free parameter that determines the strength of orientational correlations. For $A = 0$ correlations are absent, whereas large A-values corresponds to small, locally aligned filament clusters. We find that using different strengths of angular pair-correlations A does not change the negative sign of the kinetic coefficient (Supplementary Information). This implies that even a collection of pre-formed weakly aligned filaments, which collide accordingly to the experimental data p_j (Figs. 3a,b), cannot cause the system to order. It effectively augments the dealigning

contributions, causing $\overline{v}$ to decrease with increasing the magnitude of χ. We conclude that, independent of the assumptions of zero-noise and molecular chaos, the pattern formation observed in the motility assay cannot be explained solely by succession of binary filament collisions.

The transition to polar order seen in the experiment can however be understood by multi-particle collisions: Already for densities one order of magnitude below the transition density, binary collision are rare, characterised by the experimentally determined ratio $R = n_{\text{binary}}/n_{\text{all}}$ of binary collisions n_{binary} to all collisions n_{all} (Fig. 4a). At $\rho = 0.06\rho_c$ less than 10% of all collisions are binary. Thus for densities close to the transition density ρ_c, filaments predominantly encounter multi-particle collisions.

More importantly, multi-filament collisions are essential for the transition to polar order, which is manifest in the dependence of the transition density on the filament length. At a given filament density $\rho \approx 16$ filaments/μm^2, long filaments with length $L_{\text{long}} = 4 - 7\mu m$ are able to form polar structures (Fig. 4b), while an assay of short filaments with length $L_{\text{short}} = 0.5 - 3\mu m$ remain in the isotropic state (Fig. 4c). Yet, at a higher concentration $\rho \approx 30$ filaments/μm^2, short filaments are able to create clusters. At this higher concentration of filaments the long filament system is already in the density wave regime [11].

As the exact nature of the length dependence on the transition density ρ_c indicates the microscopic mechanism of the transition, we systematically vary the average filament lengths from $2 - 10\mu m$ and determine ρ_c (Fig. 4d). For a gas of propelled particles, where binary collisions are dominant (Eq.(1)), the transition density is defined by $\nu = 0$ and hence ρ_c is expected to scale with $1/L$ (see Supplementary Information Eq. (S8)). Thus, in this slender rod limit, the collision probability is determined only by the length of the collision partner. Yet, we observe here an approximately quadratic behaviour for $\rho_c(L)$ (Fig.4d), ruling out the gas-like picture for this system. At the transition density ρ_c, the total number of simultaneous collisions for a filament of length L is constant: $\rho_c L^2 \approx 200 - 300$ (Fig. 4d inset). Importantly, this implies that it is the total number of simultaneous collisions and not the filament length itself which defines the order transition.

The presented results challenge our current understanding on the polar ordering transition in active systems. Such polar ordering transition is not determined purely by the number of particles in the system but rather by the degree of multi-particle collisions. Systems governed by such features could well be described by kinetic models that incorporate collisions of arbitrary number of partners [28, 29] or goes beyond the mean-field assumption where it does not rely on Boltzmann's approximation of molecular chaos [30], which still depend on the individual interactions. The uniqueness of the actomyosin motility assay that enables the access to all microscopic interactions and parameters set a quantitative basis for further development of our understanding of ordering phenomena in this diverse class of materials.

Methods

Assay preparation

We used standard protocols to prepare the actin filaments and heavy meromyosin (HMM) motor proteins. Fluorescently labelled filaments stabilised with Alexa Fluor 488 phalloidin were used to visualise filaments with a fluorescence microscopy. Flow chambers built from nitrocellulose-coated coverslips were incubated with HMM (0.05μg/ml). BSA was used to passivate the surfaces inside the chamber after the incubation with HMM and then a dilute solution of actin filaments (binary collision: approximately 10-100nM, filament length dependency: approximately 3–10μM) was introduced. We added 2mM ATP to enable the HMM to drive the filaments and a standard antioxidant buffer supplement was used to prevent oxidation of the fluorophore. Filament length was adjusted by shearing. For details of protein and assay chamber preparations, refer to Supplementary Information.

Imaging

A Leica DMI 6000B inverted microscope was used to acquire data. A 100× oil objective (NA: 1.4) was used for the binary collision experiments and a 40× oil objective (NA: 1.25) for the filament length dependency experiment. Images of resolution 1344×1024 pixels and time resolution of 0.13 seconds were captured with a CCD camera (C4742-95, Hamamatsu) attached to a ×1 (for binary collisions) and ×0.35 (for filament length dependency) camera mount.

Data analysis

For the binary collision experiments, filaments are identified by labelling connected components in the binary images and then are skeletonised, using Matlab. A cubic spline fit is applied to the skeletonised filaments to obtain coordinates for the filament contour. The coordinates for the filament head is used to determine $\theta_{1,2}$ and $\theta'_{1,2}$. A collision is defined when two filaments touch each other, until they are separated. Any collision events involving three or more filaments are classified as non-binary. See Supplementary Information for more detail.

Supplementary Material

Refer to Web version on PubMed Central for supplementary material.

Acknowledgement

This research was supported by the European Research Council in the framework of the Advanced Grant 289714-SelfOrg, Deutsche Forschungsgemeinschaft via project No. B2 within the SFB No. 863, and the German Excellence Initiative via the program “NanoSystems Initiative Munich” (NIM).

References

[1]. Karsenti E. Self-organization in cell biology: a brief history. Nat Rev Mol Cell Biol. 2008; 9:255–262. [PubMed: 18292780]

[2]. Fletcher DA, Mullins RD. Cell mechanics and the cytoskeleton. Nature. 2010; 463:485–492. [PubMed: 20110992]

[3]. Couzin ID, Krause J. Self-organization and collective behavior in vertebrates. Adv Stud Behav. 2003; 32:1–109.

[4]. Vicsek T, Zafeiris A. Collective motion. Phys Rep. 2012; 517:71–140.

[5]. Bertin E, Droz M, Grégoire G. Boltzmann and hydrodynamic description for self-propelled particles. Phys Rev E. 2006; 74:022101.

[6]. Bertin E, Droz M, Grégoire G. Hydrodynamic equations for self-propelled particles: microscopic derivation and stability analysis. J Phys A: Math Theor. 2009; 42:445001.

[7]. Hanke T, Weber CA, Frey E. Understanding collective dynamics of soft active colloids by binary scattering. Phys Rev E. 2013; 88:052309.

[8]. Weber CA, Thüroff F, Frey E. Role of particle conservation in self-propelled particle systems. New J Phys. 2013; 15:045014.

[9]. Thüroff F, Weber CA, Frey E. Critical assessment of the Boltzmann approach to active systems. Phys Rev Lett. 2013; 111:190601. [PubMed: 24266464]

[10]. Thüroff F, Weber CA, Frey E. Numerical treatment of the Boltzmann equation for self-propelled particle systems. Phys Rev X. 2014; 4:041030.

[11]. Schaller V, Weber C, Semmrich C, Frey E, Bausch AR. Polar patterns of driven filaments. Nature. 2010; 467:73–77. [PubMed: 20811454]

[12]. Butt T, et al. Myosin motors drive long range alignment of actin filaments. J Biol Chem. 2010; 285:4964–4974. [PubMed: 19940124]

[13]. Hussain S, Molloy JE, Khan SM. Spatiotemporal dynamics of actomyosin networks. Biophys J. 2013; 105:1456–1465. [PubMed: 24047997]

[14]. Ward AJ, Sumpter DJT, Couzin ID, Hart PJB, Krause J. Quorum decision-making facilitates information transfer in fish shoals. Proc Natl Acad Sci. 2008; 105:6948–6953. [PubMed: 18474860]

[15]. Nagy M, Ákos Z, Biro D, Vicsek T. Hierarchical group dynamics in pigeon flocks. Nature. 2010; 464:890–894. [PubMed: 20376149]

[16]. Attanasi A, et al. Information transfer and behavioural inertia in starling flocks. Nature Physics. 2014; 10:691–696.

[17]. Zhang HP, Be'er A, Florin EL, Swinney HL. Collective motion and density fluctuations in bacterial colonies. Proc Natl Acad Sci. 2010; 107:13626–13630. [PubMed: 20643957]

[18]. Sumino Y, et al. Large-scale vortex lattice emerging from cocollective moving microtubules. Nature. 2012; 483:448–452. [PubMed: 22437613]

[19]. Narayan V, Ramaswamy S, Menon N. Long-lived giant number fluctuations in a swarming granular nematic. Science. 2007; 317:105–108. [PubMed: 17615353]

[20]. Aranson IS, Volfson D, Tsimring LS. Swirling motion in a system of vibrated elongated particles. Phys Rev E. 2007; 75:051301.

[21]. Kudrolli A, Lumay G, Volfson D, Tsimring LS. Swarming and swirling in self-propelled polar granular rods. Phys Rev Lett. 2008; 100:058001. [PubMed: 18352433]

[22]. Deseigne J, Dauchot O, Chaté H. Collective motion of vibrated polar disks. Phys Rev Lett. 2010; 105:098001. [PubMed: 20868196]

[23]. Vicsek T, Czirók A, Ben-Jacob E, Cohen I, Shochet O. Novel type of phase transition in a system of self-driven particles. Phys Rev Lett. 1995; 75:1226–1229. [PubMed: 10060237]

[24]. Grégoire G, Chaté H. Onset of collective and cohesive motion. Phys Rev Lett. 2004; 92:025702. [PubMed: 14753946]

[25]. Sheetz MP, Chasan R, Spudich JA. Atp-dependent movement of myosin in vitro: Characterization of a quantitative assay. J Cell Biol. 1984; 99:1867–1871. [PubMed: 6490724]

[26]. Aranson IS, Tsimring LS. Pattern formation of microtubules and motors: Inelastic interaction of polar rods. Phys Rev E. 2005; 71:050901.

[27]. Weber CA, Schaller V, Bausch AR, Frey E. Nucleation-induced transition to collective motion in active systems. Phys Rev E. 2012; 86:030901.

[28]. Ihle T. Kinetic theory of flocking: Derivation of hydrodynamic equations. Phys Rev E. 2011; 83:030901.

[29]. Ihle T. Large density expansion of hydrodynamic theory for self-propelled particles. arXiv: 1501.03570. 2015

[30]. Chou Y-L, Ihle T. Active matter beyond mean-field: Ring-kinetic theory for self-propelled particles. arXiv:1409.3161. 2014

Europe PMC Funders Author Manuscripts

Europe PMC Funders Author Manuscripts

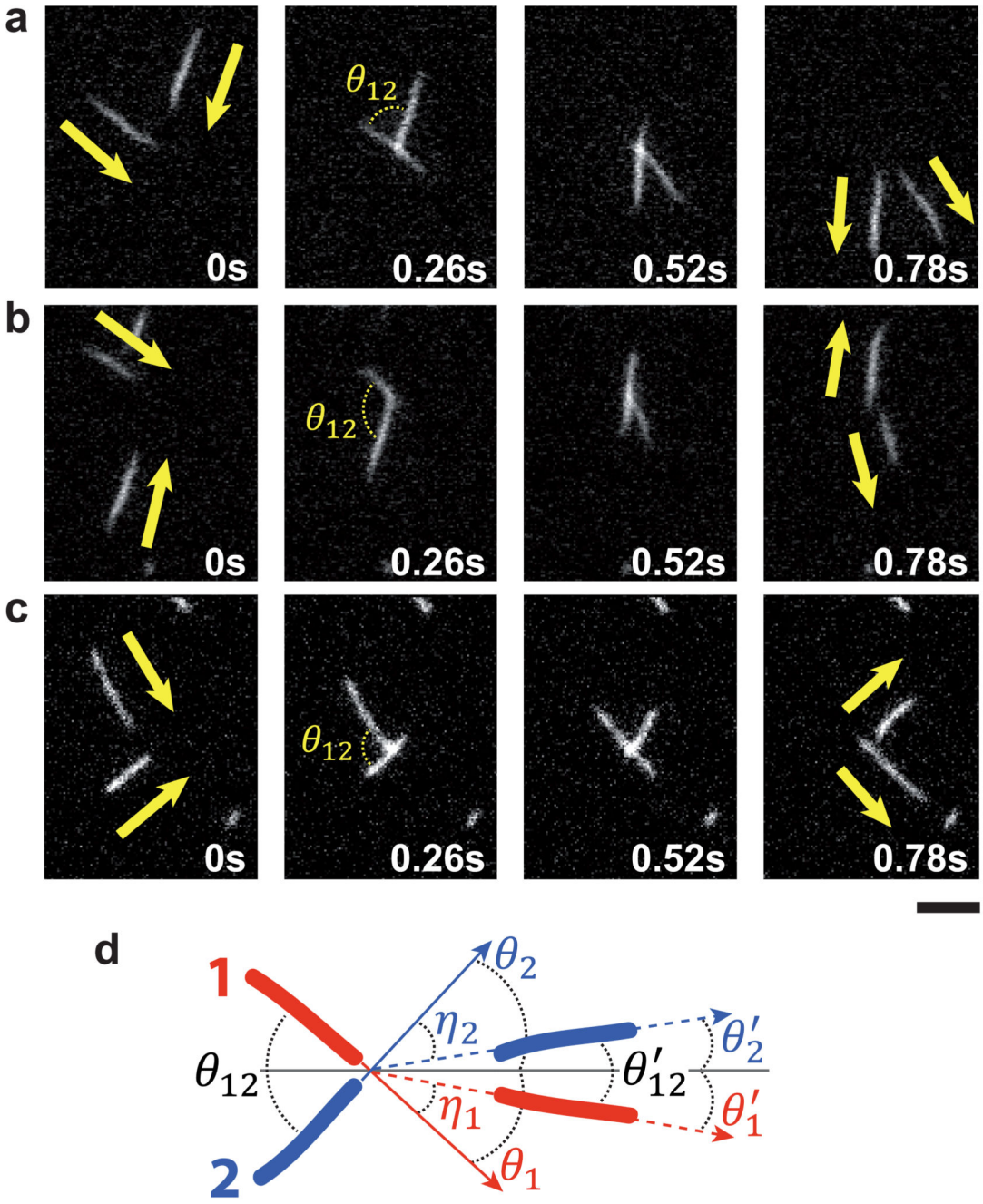

Fig. 1. Experimental binary collisions.

a-c, Time traces of representative experimental binary collisions. **a**, Polar alignment. **b**, Anti-polar alignment. **c**, Absence of alignment. Scale bar is 2μm. **d**, Definition of scattering geometry. Collisions follow the general form of $(\theta_1, \theta_2) \rightarrow (\theta_1+\eta_1, \theta_2+\eta_2)$.

Europe PMC Funders Author Manuscripts

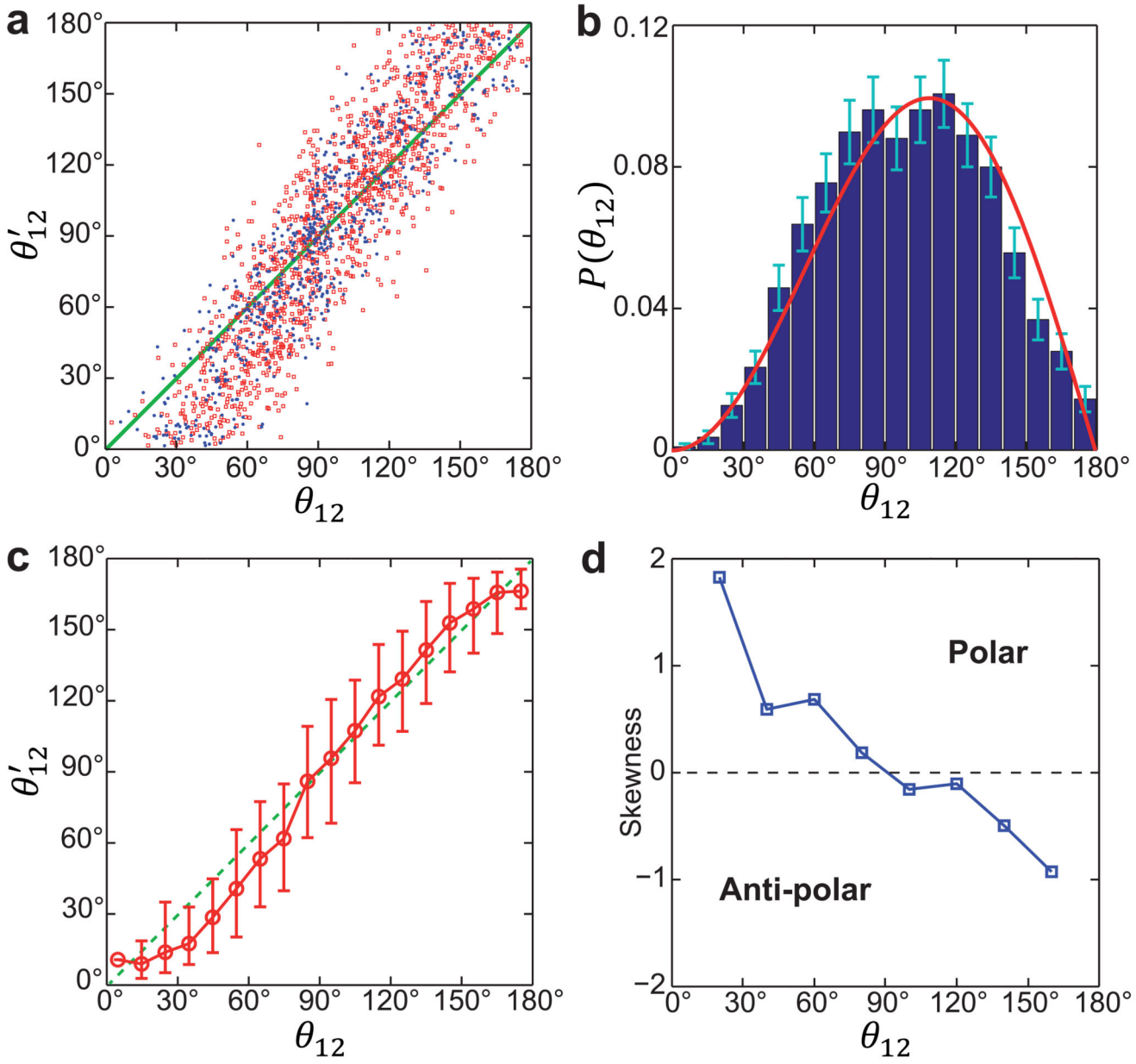

Fig. 2. Experimentally obtained binary collision statistics for the actomyosin motility assay.

a, Scatter plot of $\theta'_{12}(\theta_{12})$. Red open squares and blue solid circles represent $\rho_{low} = 0.005\rho_c$ and $\rho_{high} = 0.06\rho_c$, respectively. Green solid line represents the collisions that are unaffected ($\theta'_{12}=\theta_{12}$). Here, the numbers of collisions investigated are N_{low} = 1,113 and N_{high} = 646. **b**, Incoming angle statistics. Red solid line corresponds to the Boltzmann scattering cylinder for rods with slender rod assumption $L \gg d$. Error bars: $\pm\sqrt{N_{bin}}$. **c**, Mean plot of **a** via binning by θ_{12}. Green broken line again represents unaffected collisions. Indication of weak polar bias where $\theta'_{12}<\theta_{12}$ for highly acute θ_{12}. Error bars: Standard deviation. **d**, Skewness of θ'_{12} distribution with respect to θ_{12}. Positive and negative skewness correspond to polar

and anti-polar alignment, respectively. Skewness of 2 corresponds to an exponential distribution. In **b-d**, $\rho = \rho_{low}$.

Europe PMC Funders Author Manuscripts

Europe PMC Funders Author Manuscripts

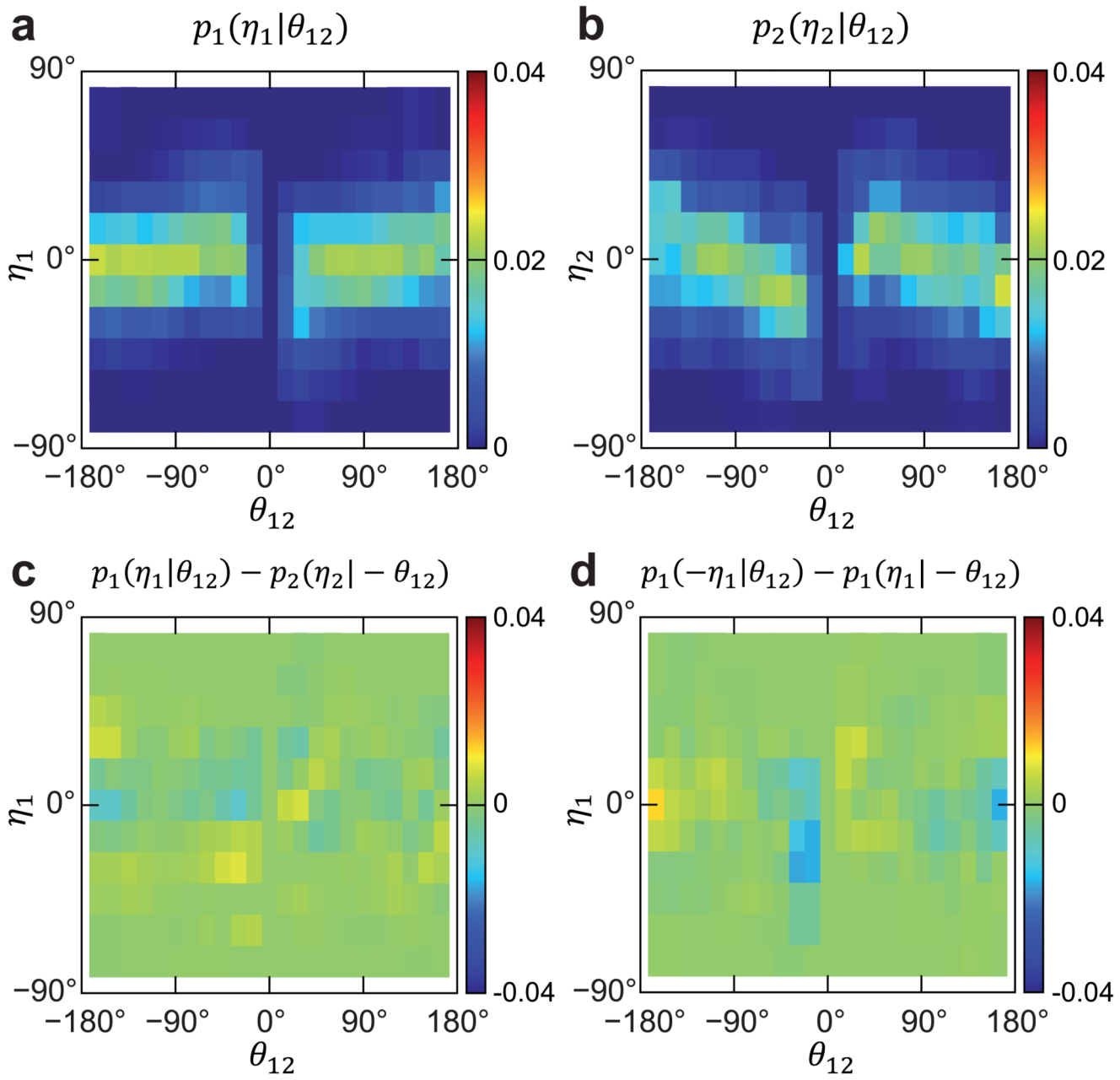

Fig. 3. Comprehensive binary collision statistics $p_j(\eta_j|\theta_{12})$ and their symmetry properties.
a,**b**, $p_1(\eta_1|\theta_{12})$ and $p_2(\eta_2|\theta_{12})$. **c**, Quantitative test of particle exchange symmetry, $p_1(\eta_1|\theta_{12}) = p_2(\eta_2| - \theta_{12})$. **d**, Quantitative check of mirror symmetry, $p_1(-\eta_1|\theta_{12}) = p_1(\eta_1| - \theta_{12})$. Binning: $\Delta\theta_{12} = 15°$ and $\Delta\eta = 15°$.

Europe PMC Funders Author Manuscripts

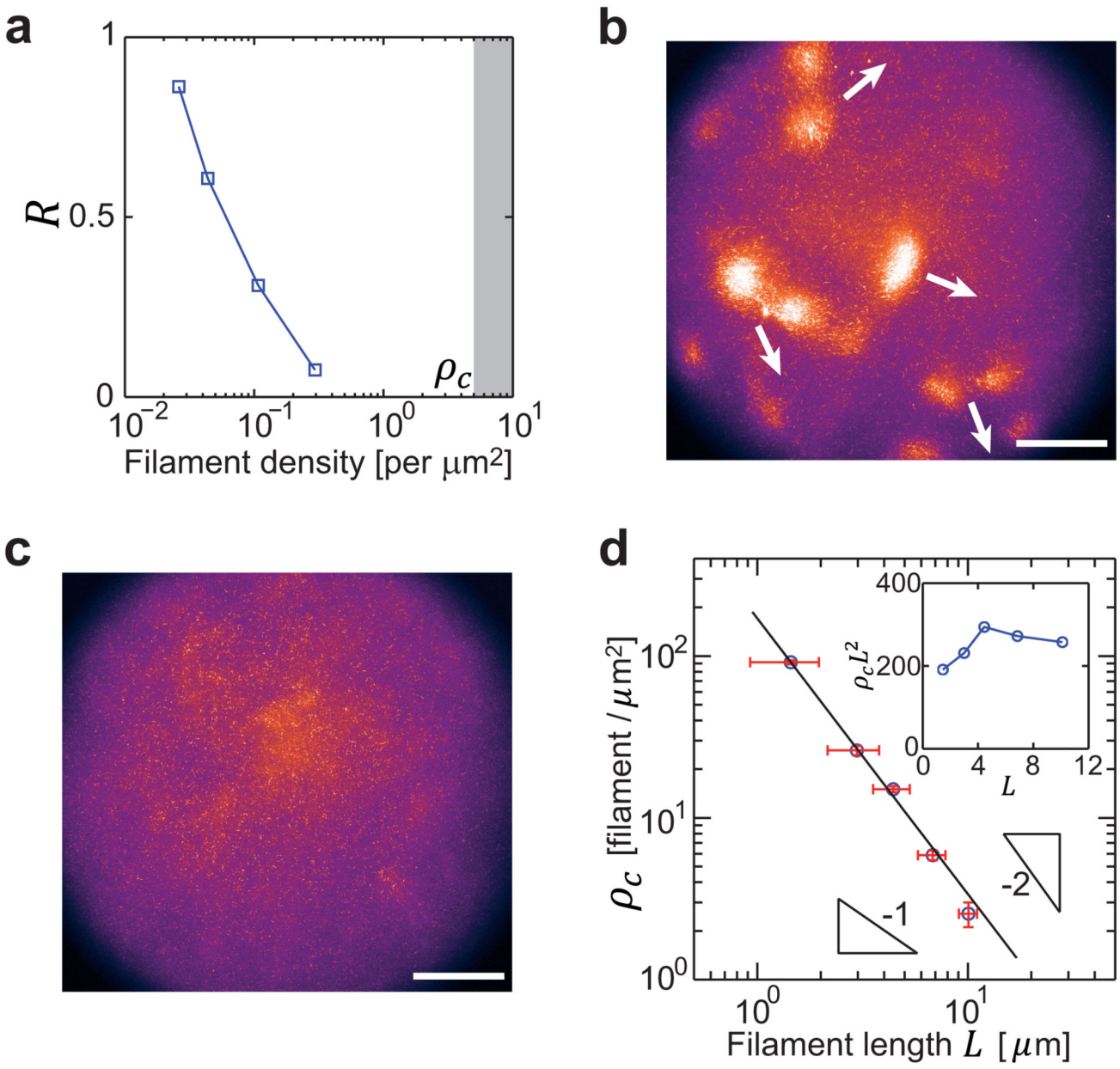

Fig. 4. Evidence of multi-filament collisions.

a, Ratio $R = n_{\text{binary}}/n_{\text{all}}$ of binary collisions n_{binary} to all collisions n_{all}. Grey zone on the right indicates the ordered phase. **b–d**, Filament length dependence on transition density ρ_c. **b**, At filament density $\rho \approx 16$ filaments/μm^2, long filaments form polar ordered active clusters. White arrows show examples of cluster motion direction. **c**, For short filaments at the same density as **b**, no polar order emerges. In **b–c**, scale bars are 100μm. **d**, Log-log plot of $\rho_c(L)$, showing an approximately quadratic dependence. Solid line shows best fit of $L^{1.71}$. Error bars: Standard deviation for both ρ_c and L. Inset: Degree of multi-filament collisions $\rho_c L^2$ against filament length L.